Journal of Vibration and Control
http://jvc.sagepub.com

Behavioral Investigation of a Nonlinear Nonideal Vibrating System

Ayman A. El-Badawy

Journal of Vibration and Control 2007; 13; 203
DOI: 10.1177/1077546307073674

The online version of this article can be found at:
http://jvc.sagepub.com/cgi/content/abstract/13/2/203

Published by:
SAGE Publications
http://www.sagepublications.com

Behavioral Investigation of a Nonlinear Nonideal Vibrating System

AYMAN A. EL-BADAWY
Department of Mechanical Engineering, Al-Azhar University, Cairo, Egypt
(abadawy@aucegypt.edu)

(Received 19 April 2006; accepted 11 September 2006)

Abstract: This work demonstrates that a simple, reduced-order, nonlinear model provides an effective analytical tool for the treatment of source-structure interactions by applying the theory to an actual structure and developing the appropriate model. The equations of motion were analyzed using perturbation analysis to determine the frequency response of the system in the vicinity of the primary resonance. The theoretical and experimental frequency response curves were compared to deduce the effective nonlinearity coefficient, and it is shown that, at certain critical speeds, the excitation source is severely limited by the structural vibrations generated.

Keywords: Nonideal system, limited power supply, Sommerfeld effect, perturbation.

1. INTRODUCTION

Almost all physical systems exhibit nonlinear phenomena and display nonideal characteristics to some extent, but in many analyses it is reasonable to assume that these effects are negligible and to model the system as linear and ideal. The influence of a vibrating system on the excitation source characterizes the degree of its nonidealness and determines whether or not the source should be included in the modeling. This investigation concentrates on modeling a system with a nonideal excitation source and provides qualitative as well as quantitive insight into the nature of nonideal interactions.

Jet engines, turbines, and automobile engines are three common examples in which the practical effects of nonideal interactions are important. Small rotating imbalances can generate large vibrations at certain system-specific critical speeds that may threaten the integrity of the supporting structure. The interaction is termed nonideal when the structure response significantly affects the ability of the source to rotate the imbalance. Because of their ease of construction and many practical applications, the study of nonideal systems has been applied primarily to rotating machines.

Though nonideal systems have been studied far less than their ideal counterparts, they have received some attention. The salient feature of such systems, which is clearly present

Journal of Vibration and Control, **13(2):** 203–217, 2007 DOI: 10.1177/1077546307073674

Figure 1 appears in color online: http://jvc.sagepub.com

in the observations discussed below, is called the Sommerfeld effect (Sommerfeld, 1904). Kononenko (1969) devoted an entire text to this subject. Nayfeh and Mook (1979) gave a comprehensive and complete review of different approaches to the problem up to 1979. More recently, De Mattos et al. (1997) presented experimental results of the vibrations excited by a rotating mass at the end of a cantilever beam. They observed that the extent of the associated jump could be increased by increasing the unbalanced mass. Also, they observed that, in some cases, the amplitude and frequency of the motion became and remained modulated. Numerical simulations (using Simulink) of a simplified model of the same problem, using an unbalanced rotor attached to an elastic nonlinear support with internal and external damping driven by a non-ideal energy source, were analyzed by Balthazar et al. (1997). Finally, Balthazar et al. (2003, 2004) presented an overview of the main properties of nonideal vibrating systems.

In this article, the experimental setup consists of a cantilevered beam supporting a large motor at its free end. Vibrations are induced by an eccentric mass on the motor shaft. This is an idealized setup that represents a simple model of a very complex system. The real system may be any machine that includes rotating equipment, such that, at certain rotational frequencies, a large vibrational response acting as an energy sink is observed within the system.

In this investigation, the supported motor reperesents the nonideal (or limited power) source of excitation, and the cantilevered beam represents the nonlinear foundation, which is analogous to the machine base or supporting structure. A nonlinear model of the system is justified because we are concerned with resonant vibrations and expect large-amplitude responses and behaviors not captured with the linear model.

In Section 2, the model is introduced and then the governing equations are identified and solved using an approximate analytic technique. In Section 3, the experimental setup and procedures are described. Discussion of the results is presented in Section 4.

2. THEORETICAL BASIS

2.1. The Model

A diagram of the experimental setup is shown in Figure 1a. Kononenko (1969) proposed the following linear beam model:

$$(m_0 + m_1)\ddot{x} + c\dot{x} + kx - m_1 r\left(\ddot{\phi}\cos\phi - \dot{\phi}^2 \sin\phi\right) = 0 \quad (1)$$

$$\left(I + m_1 r^2\right)\ddot{\phi} - m_1 r\ddot{x}\cos\phi = S(\dot{\phi}) \quad (2)$$

for a system similar to the one shown in Figure 1a. There, the overdot denotes differentiation with respect to t, and S represents the net torque of the motor. This suggests a form for our lumped parameter model. Because the system has a cantilevered beam, we expect a cubic nonlinearity. The large mass supported at the free end of the beam suggests that rotary inertia effects might also be important, so we consider modeling the system as depicted in Figure 1b. Hence, we extend Kononenko's original work and model the system as

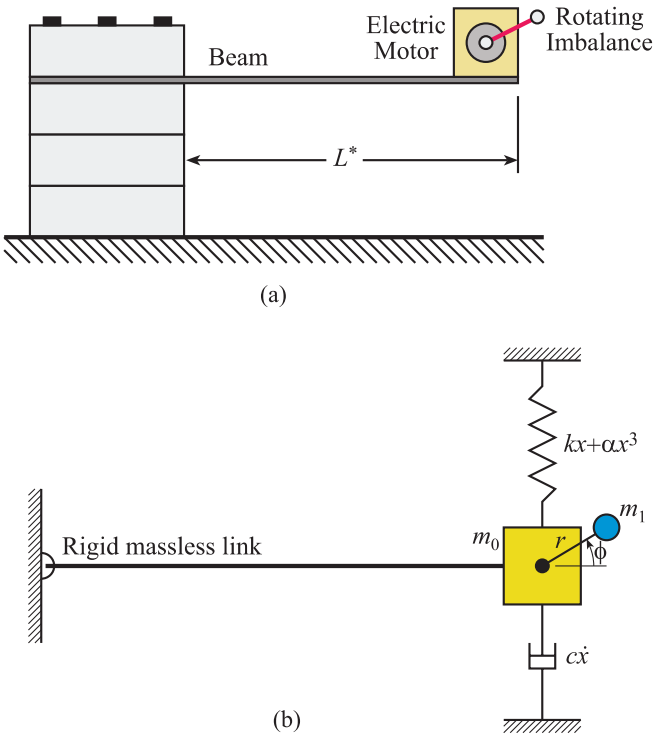

Figure 1. (a) Diagram of physical model, (b) Lumped parameter model.

$$(m_0 + m_1)\ddot{x} + c\dot{x} + kx + \alpha x^3 + \delta\dot{x}^2 x - m_1 r\left(\ddot{\phi}\cos\phi - \dot{\phi}^2\sin\phi\right) = 0 \quad (3)$$

$$\left(I + m_1 r^2\right)\ddot{\phi} - m_1 r\ddot{x}\cos\phi = S(\dot{\phi}). \quad (4)$$

Before solving equations (3) and (4), we introduce the following dimensionless variables:

$$u = \frac{x}{X} \quad \text{and} \quad \tau = \frac{t}{T}.$$

Where X and T are a characteristic length and a characteristic time, respectively. Then equations (3) and (4) can be rewritten as

$$u'' + \frac{cT}{m_0 + m_1}u' + \frac{kT^2}{m_0 + m_1}u + \alpha\frac{X^2T^2}{m_0 + m_1}u^3 + \frac{\delta X^2}{m_0 + m_1}uu'^2$$

$$- \frac{m_1 r}{X(m_o + m_1)}\left(\phi''\cos\phi - \phi'^2\sin\phi\right) = 0 \quad (5)$$

$$\phi'' - \frac{m_1 r X}{I + m_1 r^2} u'' \cos\phi = \frac{T^2}{I + m_1 r^2} S\left(\dot{\phi}\right) \tag{6}$$

where the prime denotes differentiation with respect to τ. We choose the characteristic time such that

$$\omega_0^2 T^2 = \frac{k T^2}{m_0 + m_1} = 1 \quad \text{or} \quad T^2 = \frac{m_0 + m_1}{k} \tag{7}$$

which results in a normalization of the nondimensional linear natural frequency ω_0. Additionally, for weak damping, we have

$$\frac{cT}{m_0 + m_1} = \frac{c}{\sqrt{k(m_0 + m_1)}} \equiv 2\epsilon\mu. \tag{8}$$

Finally, because the coupling between equations (5) and (6) is weak (i.e., $m_1 \ll m_0$), the nondimensional parameter

$$\epsilon \equiv \frac{m_1 r}{X(m_0 + m_1)} \tag{9}$$

is small. Thus equations (5) and (6) are rewritten as

$$u'' + 2\epsilon\mu u' + u + \frac{\alpha X^2}{k} u^3 + \frac{\delta X^2}{m_0 + m_1} u u'^2 - \epsilon\left(\phi'' \cos\phi - \phi'^2 \sin\phi\right) = 0 \tag{10}$$

$$\phi'' - \frac{m_1 r X}{I + m_1 r^2} u'' \cos\phi = \frac{m_0 + m_1}{k\left(I + m_1 r^2\right)} S\left(\dot{\phi}\right). \tag{11}$$

For the case of weak nonlinearity and small imbalance, we rewrite equations (10) and (11) as

$$u'' + 2\epsilon\mu u' + u + \epsilon\hat{\alpha} u^3 + \epsilon\hat{\delta} u u'^2 - \epsilon\left(\phi'' \cos\phi - \phi'^2 \sin\phi\right) = 0 \tag{12}$$

$$\phi'' - \epsilon b u'' \cos\phi = \epsilon \hat{S}\left(\dot{\phi}\right) \tag{13}$$

where

$$\begin{aligned} \hat{\alpha} &= \frac{X^3 (m_0 + m_1)}{m_1 k r} \alpha, \\ \hat{\delta} &= \frac{X^3}{m_1 r} \delta, \\ b &= \frac{(m_0 + m_1) X^2}{I + m_1 r^2}. \end{aligned} \tag{14}$$

2.2. Perturbation Analysis

We determine a first-order approximate solution of equations (10) and (11) using the method of averaging (Nayfeh, 1981). To this end, we apply the method of variation of parameters and let

$$u = a(\tau)\cos\left[\phi + \beta(\tau)\right] \tag{15}$$

$$u' = \frac{\mathrm{d}u}{\mathrm{d}\tau} = -a(\tau)\sin\left[\phi + \beta(\tau)\right). \tag{16}$$

We use the additional freedom we have introduced to impose the following relation:

$$u' = a'\cos(\phi+\beta) - a\left(\phi' + \beta'\right)\sin(\phi+\beta) = -a\sin(\phi+\beta). \tag{17}$$

For the case of primary resonance, we let $\phi' = 1 + \Delta$ where $\Delta \ll 1$ is a detuning parameter. Then, noting that $\phi'' = \Delta'$, and substituting equations (15) and (16) into equations (12) and (13) produces

$$\begin{aligned} & -a'\sin(\phi+\beta) - a\left(1+\Delta+\beta'\right)\cos(\phi+\beta) + 2\epsilon\mu\left(-a\sin(\phi+\beta)\right) \\ + \;& a\cos(\phi+\beta) + \epsilon\hat{\alpha}a^3\cos^3(\phi+\beta) + \epsilon\hat{\delta}a^3\cos(\phi+\beta)\sin^2(\phi+\beta) \\ - \;& \epsilon\left[\Delta'\cos\phi - (1+2\Delta)\sin\phi\right] = 0 \end{aligned} \tag{18}$$

$$\Delta' + \epsilon b\left[a'\sin(\phi+\beta) + a\left(1+\Delta+\beta'\right)\cos(\phi+\beta)\right]\cos\phi = \epsilon\hat{S}\left(\dot{\phi}\right) \tag{19}$$

where terms involving Δ^2 have been ignored. Rearranging equations (18) and (19) and combining with relation (17). Additionally, we explicitly enforce the smallness of Δ by writing $\Delta = \epsilon\sigma$, suggesting that $\phi' = 1 + \epsilon\sigma$. Thus, after some manipulation, three equations for a', β' and Δ' are obtained.

According to the method of averaging, a and β are assumed to be approximately constant over one time interval, 2π (the period of circular functions), because their variations are both of order ϵ. These assumptions allow the equations for a', β' and Δ' to be averaged in the following manner:

$$\begin{aligned} \int_0^{2\pi} a'\mathrm{d}\tau = & -\epsilon\int_0^{2\pi}\{2\mu a\sin^2(\phi+\beta) - \hat{\alpha}a^3\sin(\phi+\beta)\cos^3(\phi+\beta) \\ & - \hat{\delta}a^3\cos^2(\phi+\beta)\sin^2(\phi+\beta) - \sin\phi\sin(\phi+\beta) + O(\epsilon)\Big\}\,\mathrm{d}\tau. \end{aligned} \tag{20}$$

Which yields

$$a' \approx -\epsilon\mu a + \frac{1}{2}\epsilon\cos\beta. \tag{21}$$

The averaging approximates a by eliminating the fast-varying terms from the equation. Similarly, the averaged equations for β' and Δ' are

$$a\left(\epsilon\sigma+\beta'\right) \approx \frac{3\epsilon\hat{\alpha}}{8}a^3+\frac{\epsilon\hat{\delta}}{8}a^3+\frac{1}{2}\epsilon\sin\beta \tag{22}$$

$$\Delta' \approx -\frac{1}{2}\epsilon ba\cos\beta+\epsilon\hat{S}\left(\dot{\phi}\right). \tag{23}$$

We note the difference between ideal and nonideal systems. For the ideal system, equation (23) is not one of the governing equations, σ is specified, and equations (21) and (22) are solved for a and β. For the nonideal system, the control setting is specified, $\Delta=\epsilon\sigma$, and equations (21) through (23) are solved for σ, a, Δ, and β. The equilibrium solutions correspond to $a'=\beta'=\Delta'=0$. Hence, a, β, and $\dot{\phi}$ are given by

$$\mu a = \frac{1}{2}\cos\beta \tag{24}$$

$$\hat{S}\left(\dot{\phi}\right) = \frac{1}{2}ba\cos\beta \tag{25}$$

$$a\sigma = \frac{3}{8}\hat{\alpha}a^3+\frac{1}{8}\hat{\delta}a^3+\frac{1}{2}\sin\beta. \tag{26}$$

Equations (24) to (26) lead to the following expressions for the motor characteristics and frequency response equations:

$$\hat{S}\left(\dot{\phi}\right)=\mu a^2 b \tag{27}$$

And

$$\mu^2a^2+\left(\sigma a-\frac{3\hat{\alpha}+\hat{\delta}}{8}a^3\right)^2=\frac{1}{4}. \tag{28}$$

In terms of the physical variables, the frequency response equation is

$$c^2\left(Xa\right)^2+4\left(m_0+m_1\right)^2\left[\left(\dot{\phi}-\omega_0\right)\left(Xa\right)-\alpha_e\omega_0\left(Xa\right)^3\right]^2=\left(\omega_0 m_1 r\right)^2 \tag{29}$$

where Xa is the physical amplitude of oscillations, and α_e is the effective nonlinearity coefficient defined by

$$\alpha_e=\frac{3\alpha+\omega_0^2\delta}{8\left(m_0+m_1\right)\omega_0^2}. \tag{30}$$

Similarly, the physical equation for the torque-speed characteristic of the system is

$$L\left(\dot{\phi}\right)-H\left(\dot{\phi}\right)=S\left(\dot{\phi}\right)=\frac{1}{2}c\omega_0\left(Xa\right)^2. \tag{31}$$

Generally, it is assumed that the resisting moment $H\left(\dot{\phi}\right)$ increases linearly with the rotational speed, but we show later that it is very nearly constant in the region of interest.

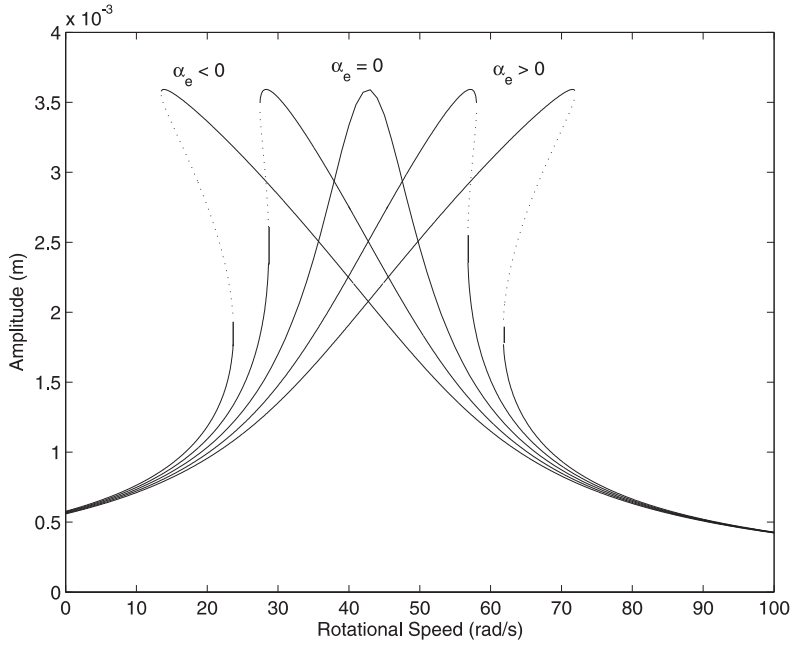

Figure 2. Theoretical frequency response of the non-ideal nonlinear system.

Therefore, subtracting $H\left(\dot{\phi}\right)$ from the torque-speed curves $L\left(\dot{\phi}\right)$ does not significantly alter the form of the curves.

2.3. Theoretical Frequency Response Curves

Figure 2 shows the effect of the beam nonlinearity α_e on the nondimensional frequency response of the system with an ideal excitation based on the real parameters of the system. If $\alpha_e = 0$, then the system behaves linearly.

When $\alpha_e \neq 0$, the frequency response curve is bent; the lower-half of the (dotted) concave portion of the curve corresponds to unstable equilibrium solutions, which are unrealizable experimentally. Systems with $\alpha_e < 0$ are called softening and those with $\alpha_e > 0$ are called hardening. Figure 2 also represents the frequency response of the load which the motor sees. These results were compared with the experimentally obtained frequency response curve to estimate the value of α_e.

The intersections of the motor characteristics $S\left(\dot{\phi}\right)$ with the system characteristics in Figure 3 represent the steady-state motions of the beam-motor system. The curve denoted as motor characteristics is obtained by solving for Xa from equation (31) knowing the actual torque-speed curve of the motor. The other curves denoted are obtained by solving for Xa from equation (29) for different values of α_e. We can now see that the jump occurs for the increasing frequency sweep when the system characteristic reaches a maximum, quickly dropping off afterwards. The motor travels along its characteristic curve in a nonstationary manner until it again intercepts the system characteristic. An analogous situation occurs for

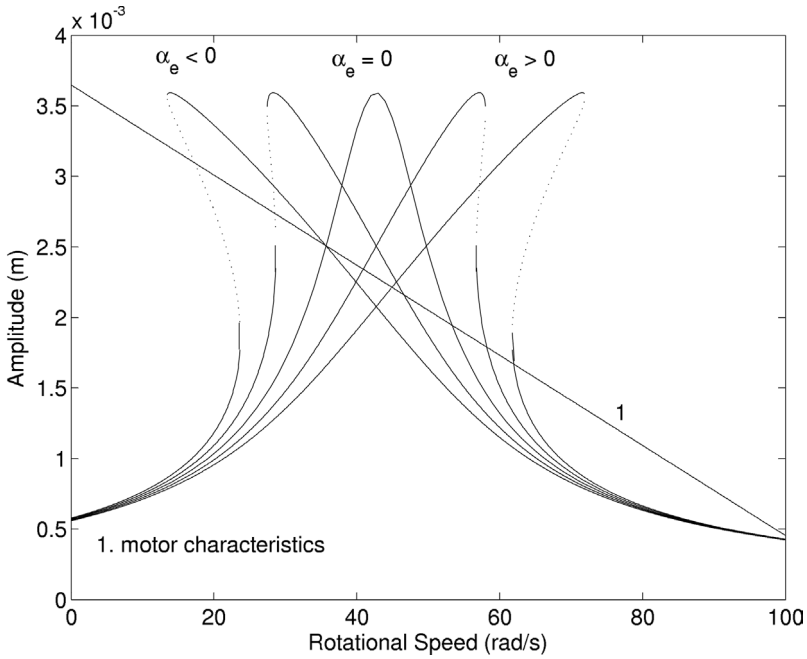

Figure 3. Expected frequency response for the system excited by a nonideal source.

the decreasing frequency sweep. Thus, we note that just as the beam nonlinearities introduced unrealizable solutions, the nonideal source affects the system in a way that causes certain states to be unrealizable.

3. EXPERIMENTS

3.1. Setup and Procedure

We analyze and discuss the nature of the full system as originally described. Before attempting this, however, we check the magnitude of the dimensionless ordering parameter ϵ. Noting that $m_0 = 5.675$ kg, $m_1 = 0.0728$ kg, and $r = 0.0268$ m, we find

$$\epsilon = \frac{m_1 r}{X\,(m_0 + m_1)} = 0.0011 \tag{32}$$

when we choose the characteristic length to be $X = L^* = 0.3$ m, which is sufficiently small.

The system consists of a motor with a rotating unbalance mounted at the end of a cantilever beam. The cantilever beam is a thin steel beam with the properties listed in Table 1.

The motor is a DC powered permanent-magnet-type motor mounted at the end of the beam. A mass is mounted on the motor shaft off the rotational axis. A tachometer is also attached to the rotor shaft by a small plastic tube acting as a flexible coupling.

Table 1. Beam Parameters.

Length	0.3 m
Young's modulus	200 GPa
Mass per unit length	1.64 kg/m
Average thickness	4.3 mm
Average width	50.6 mm

The motor was driven by a variable voltage DC supply, and the speed of the motor was varied by changing the input voltage. The operating motor provides an excitation to the system due to the presence of a rotating unbalance. The structure's response to the excitation was measured with an accelerometer. The accelerometer data was recorded in conjunction with the voltage and current supplied to the motor and the tachometer voltage output. The tachometer supplied 7V/1000rpm, so that the voltage can easily be related to the motor speed.

3.2. Results and Discussion

We started by determining the impulse and frequency response of the structure using an impact hammer. From this data, the natural frequency of the system was determined to be ≈ 6.8 Hz. The damping ratio of the system at this frequency was determined to be ≈ 0.16.

To determine the effect of the beam vibrations on the performance of the motor, we first determined its static characteristics. This was done by fixing the motor position and measuring the supplied voltage and current and the motor speed. The response of the motor was determined to be roughly linear (Figure 4a). Recall that $P_m = L\dot{\phi}$, which implies that the torque is equal to the slope of the power-speed curve. It follows from Figure (4a) that the static power-speed curve is a straight line, so the torque is constant. Because there are no applied loads, the only torque which the motor might generate at a constant speed is that needed to overcome the resistance, so $H(\dot{\phi}) =$ constant. This means that H does not affect the form of the torque-speed curves.

Next, the dynamic response of the motor was determined by releasing the beam (i.e., regular operating conditions) and measuring the motor response in the same manner in which the static motor response was determined. The motor characteristics need to be determined for both increasing and decreasing frequencies to investigate any nonlinearities of the system response. In addition, accelerometer data was taken to determine the vibration magnitudes for different operating conditions.

Figure 4b shows that, as the motor frequency approaches the frequency of the first mode, the system behavior becomes nonlinear. As the power applied to the motor increases considerably, the operating frequency of the motor remains essentially constant near, but lower than, the frequency of the first mode. Eventually, the power supplied to the motor causes the frequency to increase above the frequency of the first mode and hence the dynamic motor performance again approaches its static performance. Thus, we see a direct and very important characteristic of a system driven by a nonideal source: The inability of the source to meet specified static performance characteristics near resonance frequencies. The obvious implication of this behavior is that a motor, designed and rated in a static environment, might not be able, under realistic working conditions, to reach a desired dynamic operating frequency which is easily obtainable under static conditions. Figure 4b also shows another

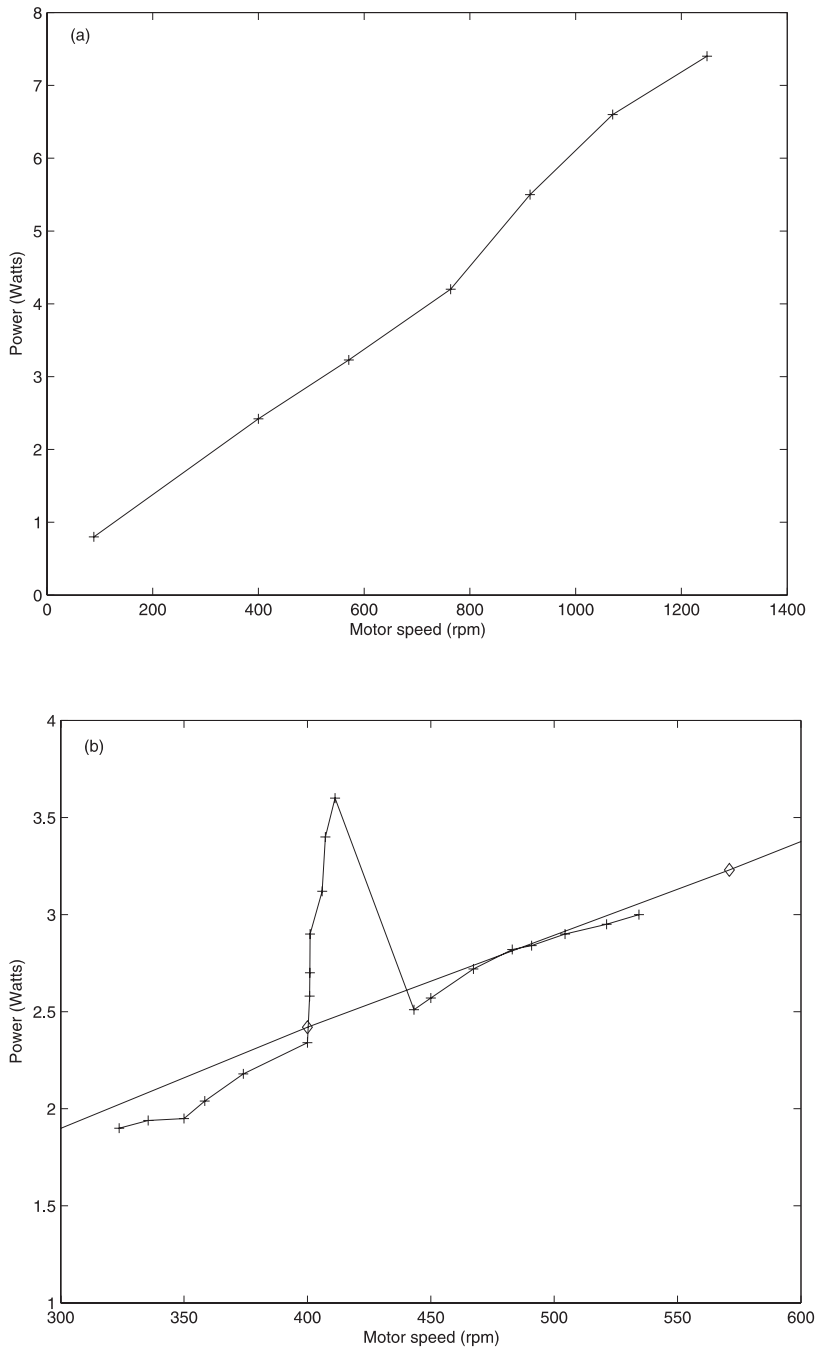

Figure 4. (a) Static performance of the motor, (b) Static and dynamic performance of the motor (overlayed).

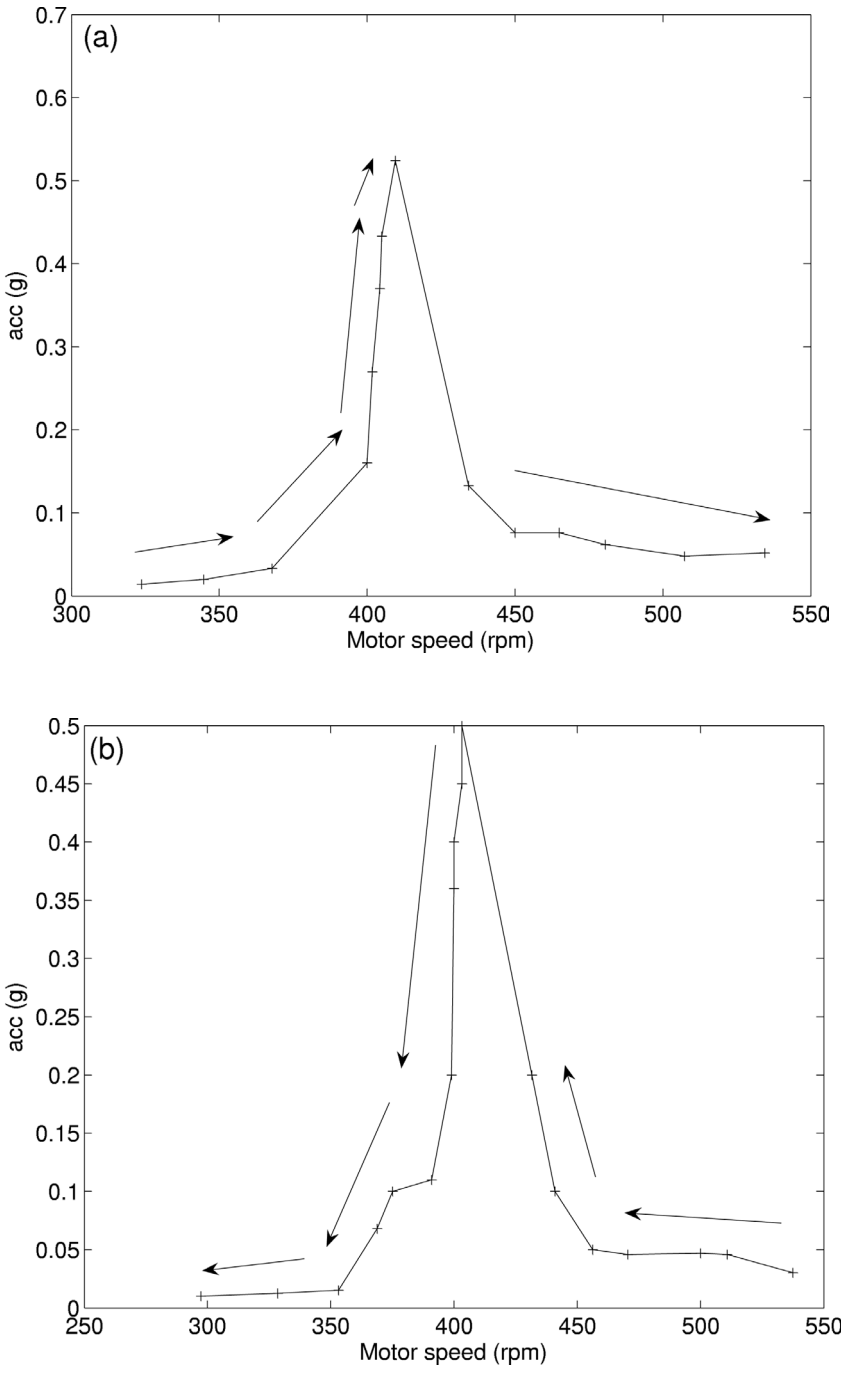

Figure 5. System response vs. motor speed: (a) increasing frequency and (b) decreasing frequency.

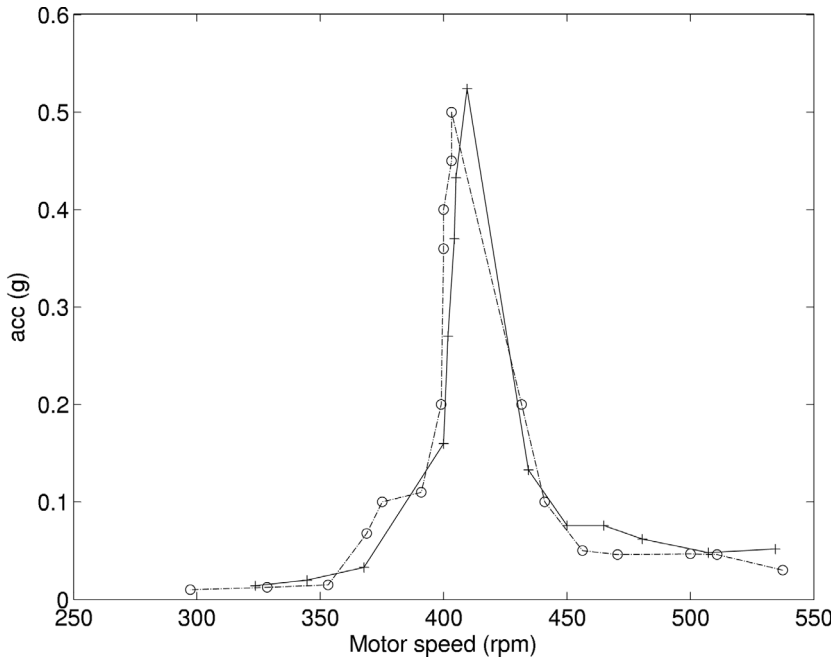

Figure 6. System response vs. motor speed: forward sweep (+) and backward sweep (o).

interesting feature in the region of resonance. As the power supplied to the motor increases, the operating frequency remains essentially constant and then suddenly increases to a value above the resonant frequency. This sudden increase in the operating frequency demonstrates the jump phenomena, which is another manifestation of the Sommerfeld effect.

Figure 5 shows the amplitude of the steady-state response against the motor speed for both increasing and decreasing driving frequencies. For the case of an increasing driving frequency, the jump changes the motor operating frequency from approximately 409 rpm to 434 rpm with no steady-state behavior observed in between. For the case of a decreasing driving frequency, the motor operating frequency jumps from approximately 431 rpm to 403 rpm. Again, no steady-state behavior was observed in the jump region. Figure 6 shows the amplitude of the steady-state response against the motor speed for increasing and decreasing frequency on the same axis. It is evident that away from resonance, the system behaves independently of the way the source is driven. When the frequency of the excitation is away from a resonant frequency, the system behaves in an ideal manner with no dependence on the direction of the frequency sweep.

To help understand the changes in the input to the motor as the system response increases, Figure 7 shows variation of the amplitude of the steady-state response plotted against the power supplied to the motor. Note the existence of multiple solutions, (i.e., that there can be two possible amplitudes for a specific power setting). The increase in the operating frequency occurs because there is a drop in the load acting on the motor. The load acting on the motor is a function of the back emf, frictional and field losses, armature losses, and external torque. All of the loads acting on the motor, with the exception of the externally

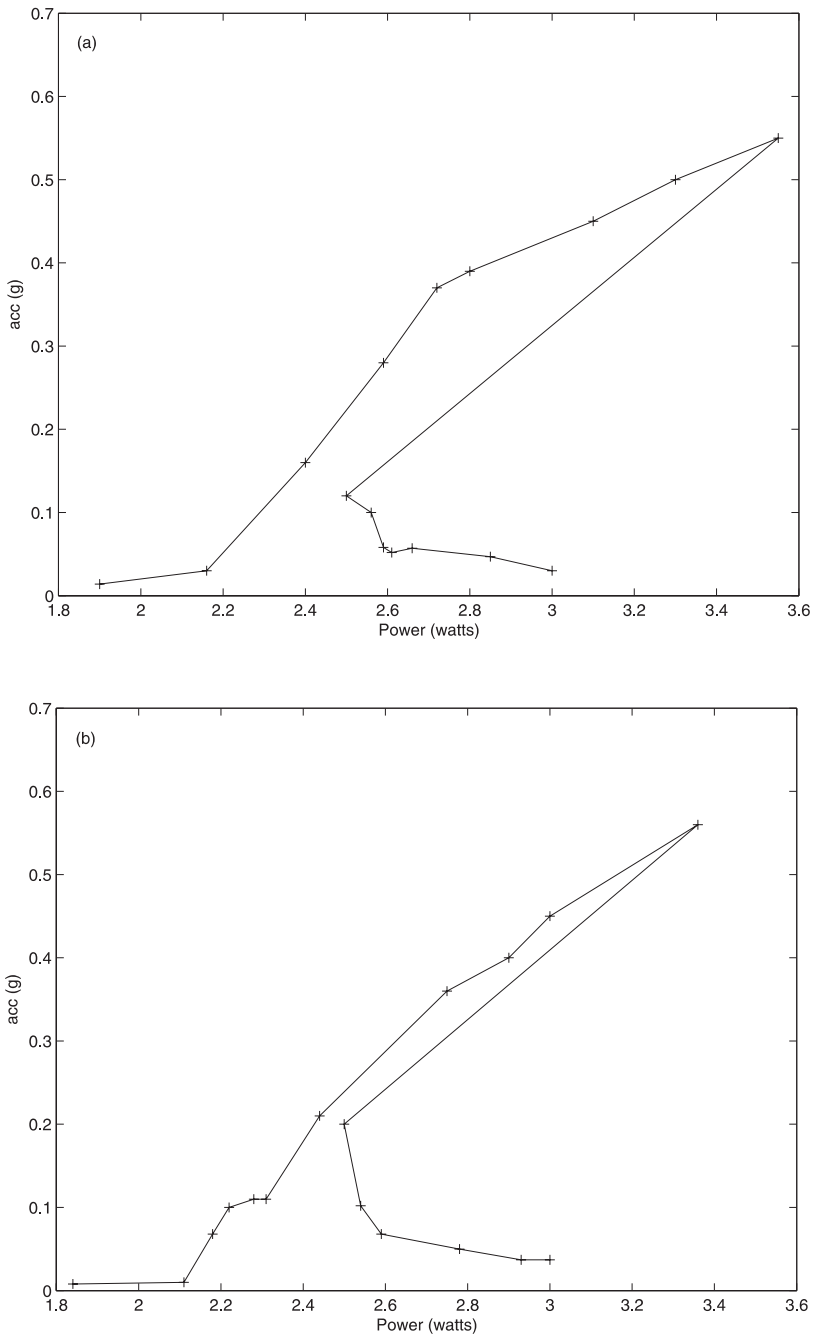

Figure 7. Power supplied to the motor vs. the steady-state response: (a) increasing frequency and (b) decreasing frequency.

applied torque, are inherent properties of the source (i.e., they define the characteristics of the source). We assume that the externally applied loads on the motor are the only torques that are affected by the response of the structure; other loads are primarily affected by the rotational speed only. The force acting on the unbalanced mass, and hence the torque acting on the motor shaft, can be seen from the equations of motion. Thus, as the system response increases, the forces acting on the unbalanced mass also increase due to the higher rpm and the fact that the unbalanced mass translates with the system; the latter has a greater effect on the total load change. Therefore, as resonance is approached, the amplitude of the response increases, causing an increase in the motor torque and so resulting in an increase in the power needed to sustain the operating speed. The net result is that a small increase in the power supplied to the motor results in a large increase in the displacement and only a small change in the motor's rotational speed. Eventually, enough power is supplied to the motor to initiate the jump, and thus the operating frequency increases and the amplitude decreases, resulting in lower power consumption by the motor.

In large systems, the time delay between the input and the response can be substantial (i.e., when power to the system is increased for purposes of changing the motor speed, the latter changes relatively slowly). In our case, the inertia is relatively small (only rotating unbalance). Thus, the motor responds essentially instantaneously to input changes. Because of the large gap in the realizable solutions near resonance, we were unable to explicitly identify the nonlinearity coefficient α_e of the system. We can, however, reach some qualitative conclusions based on our data. By comparing Figure 5 with Figure 3 we can see that α_e is near zero but negative. We know it is negative because of the way that the response becomes nearly vertical on the left, but is much more gradual on the right. We may therefore conclude that the beam nonlinearities for this system are not significant in determining the system response at the forcing levels used.

4. CONCLUSIONS

We have been able to correlate a simple, reduced-order, nonlinear model for source-structure interactions with experimental observations. Using perturbation analysis, we determined the frequency response of the system for both ideal and nonideal excitations and determined relationships among the modeled variables, which allowed us to calculate the unknown parameters of the model. Experimentally, we demonstrated the Sommerfeld effect and showed, as expected, that, at certain critical speeds, the excitation source was severly limited by the structural vibrations generated. The nonlinearity coeffecient was determined to be approximately zero.

REFERENCES

Balthazar, J.M., Mook, D.T., Weber, H.I., Brasil, R.M., Fenili, A., Belato, D., and Felix, J.L., 2003, "An overview on non-ideal vibrations", Meccanica, **38**, 613–621.

Balthazar, J.M., Mook, D.T., Weber, H.I., Brasil, R.M., Fenili, A., Belato, D., Felix, J.L., and Garzeri, F.J., 2004, "A review on new vibration issues due to non-ideal energy sources", in *Stability and Control: Theory, Methods, and Applications*, F.E. Udwadia, H.I., Weber and G. Leitman (eds), Vol. 22, pp. 237–258, Taylor and Francis, London.

Balthazar, J.M., Rente, M.L., Mook, D.T., and Weber, H.I., 1997, "Some observations on numerical simulations of a non-ideal dynamical system", in *Nonlinear Dynamics, Chaos, Control and Their Applications to Engineering Sciences*, J.M. Balthazar, D.T. Mook and J.M. Rosario (eds), Vol. 1, pp. 88–96.

De Mattos, M.C., Balthazar, J.M., Wieczork, S., and Mook, D.T., 1997, "An experimental study of vibrations of non-ideal systems", in *Proceedings of DETC'97, ASME Design Engineering Technical Conference*, September 14–17, Sacramento, CA, CD-ROM.

Kononenko, V.O., 1969, *Vibrating Systems with a Limited Power Supply*, Illife Books, London.

Nayfeh, A.H., 1981, *Introduction to Perturbation Techniques,* Wiley, New York.

Nayfeh, A.H. and Mook, D.T., 1979, *Nonlinear Oscillations*, Wiley, New York.

Sommerfeld, A., 1904, (in German) *VDI Zeitschrift*, **48**, 631–636.